Atmospheric
Measurement
Techniques

A high-altitude balloon platform for determining exchange of carbon dioxide over agricultural landscapes

Angie Bouche[1], Bernhard Beck-Winchatz[2], and Mark J. Potosnak[1]

[1]Department of Environmental Science and Studies, DePaul University, 1110 W Belden Ave,
Chicago, IL, 60614, USA
[2]Department of Science, Technology, Engineering and Math Studies, DePaul University,
990 W Fullerton Ave, Chicago, IL, 60614, USA

Correspondence to: Mark J. Potosnak (mpotosna@depaul.edu)

Abstract. The exchange of carbon dioxide between the terrestrial biosphere and the atmosphere is a key process in the global carbon cycle. Given emissions from fossil fuel combustion and the appropriation of net primary productivity by human activities, understanding the carbon dioxide exchange of cropland agroecosystems is critical for evaluating future trajectories of climate change. In addition, human manipulation of agroecosystems has been proposed as a technique of removing carbon dioxide from the atmosphere via practices such as no-tillage and cover crops. We propose a novel method of measuring the exchange of carbon dioxide over croplands using a high-altitude balloon (HAB) platform. The HAB methodology measures two sequential vertical profiles of carbon dioxide mixing ratio, and the surface exchange is calculated using a fixed-mass column approach. This methodology is relatively inexpensive, does not rely on any assumptions besides spatial homogeneity (no horizontal advection) and provides data over a spatial scale between stationary flux towers and satellite-based inversion calculations. The HAB methodology was employed during the 2014 and 2015 growing seasons in central Illinois, and the results are compared to satellite-based NDVI values and a flux tower located relatively near the launch site in Bondville, Illinois. These initial favorable results demonstrate the utility of the methodology for providing carbon dioxide exchange data over a large (10–100 km) spatial area. One drawback is its relatively limited temporal coverage. While recruiting citizen scientists to perform the launches could provide a more extensive dataset, the HAB methodology is not appropriate for providing estimates of net annual carbon dioxide exchange.

Instead, a HAB dataset could provide an important check for upscaling flux tower results and verifying satellite-derived exchange estimates.

1 Introduction

The exchange of carbon dioxide between the atmosphere and the biosphere is a crucial link in the global carbon cycle. Interactions between the biosphere and atmosphere take place in this cycle through the processes of photosynthesis and respiration. Humans perturb this cycle by releasing carbon dioxide through anthropogenic activities. Annually (2000–2009), there was a release of 7.8 PgC as carbon dioxide attributed to the combustion of fossil fuels and cement production (Ciais et al., 2013). Through photosynthesis, the terrestrial biosphere is currently taking in excess carbon dioxide from the atmosphere and therefore increasing its carbon content. Analysis of the annual global carbon cycle has found that approximately half of the anthropogenic carbon dioxide released remains in the atmosphere, while the rest dissolves in ocean water or is incorporated into plant biomass. Another human perturbation in the global carbon cycle is the appropriation of photosynthesis through agriculture and other land management practices. This appropriation is estimated at 14.8 PgC or 25 % of global net primary productivity in 2005, and croplands account for about half of total appropriation (Krausmann et al., 2013). Agricultural landscapes also make up a large portion of the biosphere, so the interactions between crops and atmospheric carbon dioxide is key

for understanding the global carbon cycle. This has led to an interest in understanding the impact of agricultural practices, such as no-tillage, on the net carbon balance of agricultural systems, but experimental results are often conflicting (Luo et al., 2010) and point to the need for diverse measurement strategies of the carbon balance of agricultural landscapes.

Measuring the net ecosystem exchange (NEE) of carbon dioxide for agroecosystems can show whether agricultural practices are an effective way to offset some of the carbon dioxide that was released into the atmosphere through anthropogenic causes. Considering annual crops, agricultural practices that increase soil organic carbon (SOC) remove carbon dioxide from the atmosphere (here defined as negative NEE), neglecting any carbon flows through hydrological systems. While there is debate about the effectiveness of no-tillage farming (Hollinger et al., 2005; Luo et al., 2010), cover crops are another method being considered for increasing SOC (Poeplau and Don, 2015). The effectiveness of these practices can be constrained by measuring the NEE of carbon dioxide between agricultural systems and the atmosphere. Surface–atmosphere exchange measurements complement methodologies that assess the change in SOC to determine agroecosystem carbon balance. A variety of strategies have been employed to measure carbon dioxide fluxes in an effort to understand these exchanges.

Data collected with towers, satellites and airplanes have been used to quantify fluxes of carbon dioxide. The eddy covariance (EC) approach employs instruments mounted on towers to measure NEE over areas on the order of $1 \, \text{km}^2$ (Monson and Baldocchi, 2014). In combination with chemical tracers, these flux measurements can be used to infer anthropogenic and biogenic influences on carbon dioxide mixing ratios over wider areas (Potosnak et al., 1999). However, there is not a large amount of data available that measure carbon dioxide exchanges in agricultural areas using this technique (Barcza et al., 2009). Surface measurements of carbon dioxide mixing ratio from a global network can be combined with atmospheric transport models and a priori estimates of anthropogenic and oceanic carbon dioxide exchanges to produce regional estimates of biotic carbon dioxide exchange (Enting et al., 1995; Gurney et al., 2002). These efforts have produced important results at the regional scale (Peters et al., 2007), but they do rely on an imperfect measurement network, estimated a priori sources and complex transport models (Gurney et al., 2004).

Collecting data via satellites and performing inverse models is another way to measure carbon dioxide fluxes over areas of land on the order of $10^7 \, \text{km}^2$, but again there is not a large body of data available and there are significant measurement uncertainties (Reuter et al., 2014). Progress is being made by using satellite data to constrain carbon dioxide exchanges at the scale of large urban areas, but efforts currently focus on atmospheric mixing ratio enhancements and not exchanges (Schneising et al., 2013). New approaches using solar-induced fluorescence derived from satellite mea-

surements to predict crop productivity are promising (Guan et al., 2016), but these will require validation. An alternative approach is to perform a budget of carbon dioxide in the mixed layer. With some assumptions, the surface flux of carbon dioxide can be calculated from vertical profiles of carbon dioxide mixing ratio in the mixed layer.

This long-standing technique was employed with aircraft in the Amazon during the 1980s (Wofsy et al., 1988), and the theory was thoroughly considered during the 1990s (Denmead et al., 1996). Measurement efforts using aircraft continue (Chou et al., 2002; Martins et al., 2009), along with further advances in theoretical treatment (Laubach and Fritsch, 2002). While the technique is robust, the expense of aircraft is considerable. An alternative involves carbon dioxide sensors flown on high-altitude balloons (HABs). Given assumptions detailed below, HABs can measure surface exchange by comparing mixing ratio profiles between two sequential flights and performing a mass-balance calculation. HABs are able to collect data at an intermediate scale between the small-scale measurements collected by towers and large-scale measurements collected using satellites. The spatial scale is similar to aircraft measurements (Mays et al., 2009), but the cost is much lower. This paper describes flying an in situ instrument, but another proposed technique that could use HABs is AirCore. This simple sampling device is also low cost and has been tested with an aircraft platform (Karion et al., 2010). Some drawbacks to the mixed-layer budget approach are limited temporal resolution and the requirement of spatial homogeneity.

Satellite vegetation indices related to the chlorophyll content of plants have been used to interpret and assess NEE surface-exchange measurements in many studies: for example, from tall towers near croplands (Barcza et al., 2009) and multi-site meta-analyses (Churkina et al., 2005). NDVI values are also used as inputs to continental-scale carbon cycle models because their seasonal variations track the amount of carbon dioxide plants take in through photosynthesis (Sims et al., 2008). Some caution is necessary, because NDVI is not always an accurate predictor of crop yields, and in some cases predictions based on NDVI measurements indicate lower crop yields than what was actually grown (Mkhabela et al., 2005). As another example, NDVI values were inferred to point to net carbon sinks in irrigated croplands and temperate forests across the United States (Potter et al., 2007). However, Sus et al. (2013) found variations in carbon dioxide uptake depended on land management and sowing field dates. These factors of uncertainty lead to NEE predictions that did not differ significantly from carbon neutrality. In spite of these limitations, there is often a strong temporal correlation between NDVI and NEE that can serve as a constraint for assessing the quality of HAB measurements. During the spring and early summer when crops are growing, NDVI increases as crops leaf out and leaf chlorophyll content increases. In the summer, crops are fully expanded and NDVI reaches a maximum value. In fall, crops are left in the field to dry, and

NDVI decreases throughout this process as leaf chlorophyll content decreases during senescence. In the winter after harvest, NDVI is lowest since bare ground is exposed. These seasonal trends should mirror trends in NEE. Moving from spring to summer, NEE becomes negative because crops are growing and photosynthesis exceeds total respiration. NEE is most negative in the middle of summer when plants are conducting photosynthesis rapidly. When crops are left in the field to dry or are harvested, NEE is expected to be positive because crops are not conducting photosynthesis or growing, while the soil is still respiring.

To assess the quality of NEE measured with the HAB platform, 2 years of growing-season results are compared to the satellite-derived NDVI values from an area representative of the HAB footprint. Based on the argument outlined in the previous paragraph, we hypothesized that the HAB NEE values should follow the same seasonal pattern as NDVI if the method is effective. In addition, the magnitude of the NEE values measured with the HAB platform are compared to publicly available data from a EC flux site.

2 Materials and methods

Measuring NEE can be accomplished by comparing vertical profiles of carbon dioxide mixing ratios from two HAB launches 3–4 h apart. We followed the fixed-mass column approach outlined by Laubach and Fritsch (2002). Compared to using the variable mixed-layer height, this approach has some advantages for calculating the contribution of entrainment in the budget, because there are fewer assumptions about the structure and evolution of the vertical profile of carbon dioxide in the free troposphere. The technique is based on estimating the boundary layer height for both flights and also considering changes in the density of the air column. The mass of the column is calculated by integrating air density from the surface to both the initial and the final boundary layer heights. The larger of these two masses is then selected for the budget, which is typically the mass of the final flight during conditions when the mixed-layer height is growing. If there is little or no observable growth, the initial flight can have the larger mass since thermal expansion of the mixed layer leads to lower densities for the final flight. This calculated mass is then used for both flights (Laubach and Fritsch, 2002, Eqs. 30 and 31). With the fixed mass, the column exchange of carbon dioxide (including entrainment but not subsidence) is then calculated by comparing the vertical spatial average of the carbon dioxide mixing ratios between the two flights (Eq. 33 in Laubach and Fritsch and also included in Eq. 2 below). When the average carbon dioxide mixing ratio is higher for the first flight than the second, carbon dioxide is being removed from the atmosphere (defined as negative NEE and corresponding to photosynthesis exceeding respiration). Similar to the EC technique, this method assumes that net horizontal advection is negligible and therefore requires
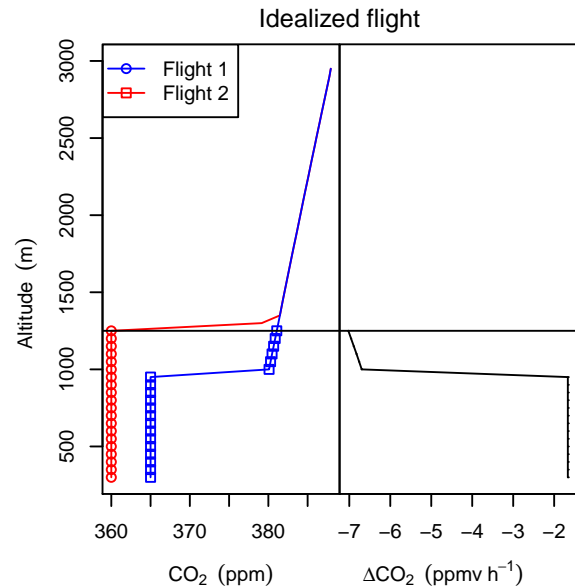
Figure 1. An idealized flight that includes a well-mixed, homogeneous mixing ratio of carbon dioxide near ground level, then a decrease in carbon dioxide mixing ratio from the first launch (blue) to second launch (red) corresponding with an increase in the boundary layer height. Above the boundary layer height of the second flight, mixing ratios between the flights should match again because ground-level photosynthetic activity does not affect carbon dioxide mixing ratios above this altitude (left panel). Both the decrease in the mixed-layer carbon dioxide mixing ratio and the increase in the boundary layer height contribute to ΔCO_2, and hence NEE. This idealized picture neglects subsidence and horizontal advection.

spatial homogeneity across the area being studied. To put a practical limit on the assumption of horizontal homogeneity, the relevant changes in carbon dioxide are assumed to be in the boundary layer, which is defined as the layer of the troposphere affected by surface exchanges within a timescale of 1 h or less (Stull, 1988). The method does rely on a knowledge of the boundary layer height. During the daytime in the summer, the atmosphere is approximately homogeneous in its carbon dioxide mixing ratio within the boundary layer because it is mixed by convection and turbulence (the mixed layer; Stull, 1988). Above the mixed layer, at an altitude of approximately 1000–2000 m, there is a large increase in carbon dioxide mixing ratio over a relatively short change in altitude (the entrainment zone) that can be visually identified. The mixed-layer height typically increases for the second flight due to increased vertical mixing driven by additional solar heating at the surface (Fig. 1). Above the mixed-layer height, the two carbon dioxide profiles should be similar, and differences would be due to changes in large-scale horizontal advection and subsidence.

The current procedure is a modification on a previous method (Pocs, 2014), where one balloon launch was conducted per day and NEE was calculated based on the dif-

ference in carbon dioxide values recorded during the ascent and descent of a single flight. In the previous methodology, the launch site and retrieval site could have different surface characteristics that could affect carbon dioxide mixing ratios in the surface layer. Therefore, using two ascents for comparison removed an aspect of spatial heterogeneity. The additional time between flights, when compared to the time between ascent and descent of a single flight (less than 1 h), also allowed for a larger difference in carbon dioxide mixing ratio and a greater increase in the boundary layer height.

Throughout the summers of 2014 and 2015, a total of 10 launches were performed. Four of these launches took place from July to September 2014, and six took place from June to September 2015 (Table 1). As the balloon ascended, burst and descended, it was followed by a chase vehicle using GPS location data received from the tracking devices. Once the balloon was retrieved, the process was repeated approximately 3 h later. The launches took place at an athletic field at Pontiac Township High School in Pontiac, IL (40.886° N, 88.616° W), with the exception of the flight on 17 July 2014, which took place at Koerner Aviation in Kankakee, IL (41.096° N, 87.913° W). Both of these locations were small towns surrounded by agricultural fields of soy and corn crops, broken into the typical pattern of $2.6 \, km^2$ sections.

The equipment launched during each flight (Fig. 2) consisted of a latex balloon filled with helium, a parachute, two GPS tracking devices, a carbon dioxide sensor and an ozone sensor (2015 flights only). The ozone data were collected for another project to measure surface ozone exchange. The parachute (Rocketman Enterprise, Inc., Bloomington, MN, USA) had a spreader (wooden ring) and was above the Stratostar GPS command module (Noblesville, IN, USA). The command module was the primary source for tracking the location of the balloon, including the altitude provided by GPS. It also collected data on pressure, which was used to align the carbon dioxide data to the Stratostar GPS data. These data were relayed in real time to the chase vehicle via a 900 MHz radio signal. Carbon dioxide molar mixing ratios (ppmv) were obtained with a LICOR LI-820 (Lincoln, NE, USA). Ambient air was pumped through an air filter and then the carbon dioxide measuring device. The instrument was powered by 10 lithium AA disposable batteries. The instrument also reported cell pressure and temperature (controlled to 50 °C). Because of the relatively slow flow rate ($< 1 \, L \, min^{-1}$) and lack of restriction on the instrument outlet, cell pressure was assumed to be equal to ambient pressure. The LI-820 is an infrared gas analyzer (IRGA), and therefore directly measures the optical absorptance of carbon dioxide in the cell. The instrument's software uses the measured cell pressure and the assumption of a controlled temperature to convert absorptance to a mixing ratio (i.e., mole fraction). The air was not dried, so there is some error introduced if humidity changes between the flights (see error analysis). On the 19 June, 2 and 15 July 2015 flights, a LICOR LI-840 was
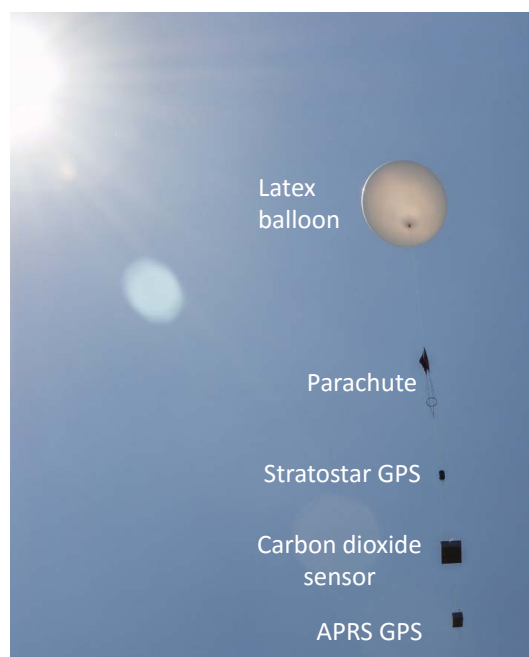
Figure 2. Picture of flight train of packages. The total package weight of 5.4 kg was lifted by a 200 g latex balloon that was filled with industrial-grade helium. The packages were all connected with 1.8 m lines (mason's string), except for 5.5 m lines for the balloon to parachute connection.

used. This instrument enabled us to also measure water vapor mixing ratios, which were used to understand the structure of the boundary layer and the impact of water vapor dilution. The two IRGAs were calibrated for carbon dioxide with a zero and a two-point calibration. After the instrument was zeroed, the higher calibration standard (510.0 ppmv) was used to set the span, and then the calibration was checked with the lower calibration standard (372.4 ppmv). Standards were obtained from Airgas Specialty Gases (Chicago, IL, USA).

The data were collected from the LICOR instrument serial output using an Arduino (http://www.arduino.cc/) microcontroller system and a memory card. A backup analog data logger (HOBO U12, Onset, Bourne, MA, USA) that recorded only carbon dioxide and pressure from the LICOR was also used. Finally, another GPS tracker (BigRedBee, Lake Oswego, OR, USA) was attached to the LICOR flight package and was used as a secondary tracking device that sent location data via a network of amateur ham radio operators to a website (Automatic Packet Reporting System, http://aprs.org/).

Prior to each launch date, the flight paths were predicted using the Cambridge University Spaceflight Landing Predictor (http://predict.habhub.org/), which uses winds generated by the NOAA GFS (National Oceanic and Atmospheric Administration Global Forecast System) model (Fig. 3). For 2014 launches, a 200 g latex balloon (Kaymont Consolidated Industries, Deer Park, NY, USA) was filled with industrial

Table 1. Flight data from all flights conducted during the summers of 2014 and 2015. Each date had two separate flights to produce one estimate of NEE.

Date	Burst altitude 1 (m)	Ascent rate 1 (m s^{-1})	Burst altitude 2 (m)	Ascent rate 2 (m s^{-1})
17 Jul 2014	14 770	4.99	13 480	6.75
14 Aug 2014	15 000	5.16	14 810	5.49
21 Aug 2014	14 760	6.04	15 530	6.24
19 Sep 2014	13 290	6.34	13 850	5.52
19 Jun 2015	14 200	4.70	13 060	4.81
02 Jul 2015	13 030	5.37	13 730	5.10
15 Jul 2015	12 340	6.07	13 450	5.89
23 Jul 2015	12 930	5.93	12 490	6.40
13 Aug 2015	13 810	6.40	13 200	6.38
12 Sep 2015	9040	6.21	9400	5.21

grade helium until it obtained approximately 5 kg of lift, which produced an initial ascent rate of approximately 5–6 m s^{-1} for our payload weight of 3.6 kg. In 2015, the balloon was filled until it obtained 7–8 kg of lift. It was necessary to obtain more lift on 2015 launches because an extra ozone sensor (1.8 kg) was attached to the flight package, giving a total weight of 5.4 kg. On the 12 September 2015 flight, a 150 g balloon was used. Typically the balloons reached an altitude of around 13 000–15 000 m before bursting, but by using the smaller 150 g balloon on the 12 September 2015 flight the burst altitude was reduced to approximately 9000 m (Table 1).

The data were analyzed using R (version 3.3.1, R Core Team, 2016). To calculate a surface exchange from the measured carbon dioxide profiles, the fixed-mass column approach was applied. Some simplifications were employed due to the nature of the low-cost, low-weight flight package. The errors associated with this simplified approach are considered in Sect. 3. All data were averaged by altitude into 50 m bins with the first bin at 300–350 m (the launch sites were at an elevation of approximately 230 m; everything referenced to height above mean sea level) and the last bin at 2950–3000 m.

Because air temperature (T, K) is required for the fixed-mass column approach to find the air density (ρ, kg m^{-3}) but was not directly measured with the low-cost flight package, we computed the potential temperature (Θ) under the assumption that potential temperature was constant in the mixed layer. The profile of pressure (P, Pa) vs. the GPS-estimated altitude (z, m) was used to calculate potential temperature and also the altitude ($z_\circ$), where air pressure was equal to 100 kPa ($P_\circ$). Combining the definition of potential temperature ($\Theta = T \left(\frac{P_\circ}{P} \right)^{R/C_P}$) and the ideal gas law ($P = \rho RT$), the hydrostatic equation ($dP = -\rho g \, dz$) was integrated to find

$$z = \Theta \times \underbrace{\frac{C_P}{g} \left[\left(\frac{P}{P_\circ} \right)^{R/C_P} - 1 \right]}_{\text{Scaled pressure}} + z_\circ, \tag{1}$$

with the constants R, C_P and g being the ideal gas constant for dry air (287 J kg^{-1} K^{-1}), the specific heat capacity for dry air at constant pressure (1004 J kg^{-1} K^{-1}) and the acceleration due to gravity (9.81 N kg^{-1}), respectively. This equation can also be derived from the definition of potential temperature and assuming the dry adiabatic lapse rate. By scaling the observed pressure as indicated by the equation, a linear fit between the altitude and the scaled pressure gives the potential temperature as the slope and the altitude where pressure is 100 kPa as the intercept. Using the calculated potential temperature and the average measured pressure, the density of air was found using the ideal gas law for each altitude bin.

Next, the integrated ground exchange between the two flights was calculated according to Eq. (43) in Laubach and Fritsch (2002), using the notation from that paper:

$$I_S^G = \alpha_S \tag{2}$$
$$\left\{ M_{\text{top}} \left(\langle s \rangle_{\text{top2}} - \langle s \rangle_{\text{top1}} \right) + \frac{1}{2} w_{\text{top}} \rho_{\text{top}} \left(\Delta s_2 + \Delta s_1 \right) \left(t_2 - t_1 \right) \right\},$$

where I_S^G is the integrated ground flux (μ mol m^{-2}), α_S converts from mass to mole units (mol kg^{-1}), M_{top} is the constant mass of the column (kg), $\langle s \rangle_{\text{top1,2}}$ is the spatially averaged mixing ratio of carbon dioxide at the beginning and end of the integration (ppmv), w_{top} is the vertical velocity due to synoptic-scale meteorology (m s^{-1}), ρ_{top} is the air density at the top of the column, Δs is the difference between the mixing ratio above the column and average column mixing ratio $\left(s_{\text{top}} - \langle s \rangle_{\text{top}} \right)$ and $(t_2 - t_1)$ is the change in time (s). The angle operator ($\langle \, \rangle$) denotes the vertical spatial average from 300 m to the top of the fixed-mass column.

Each of the terms in Eq. (2) were determined from the profiles of density and carbon dioxide mixing ratio. In a slight
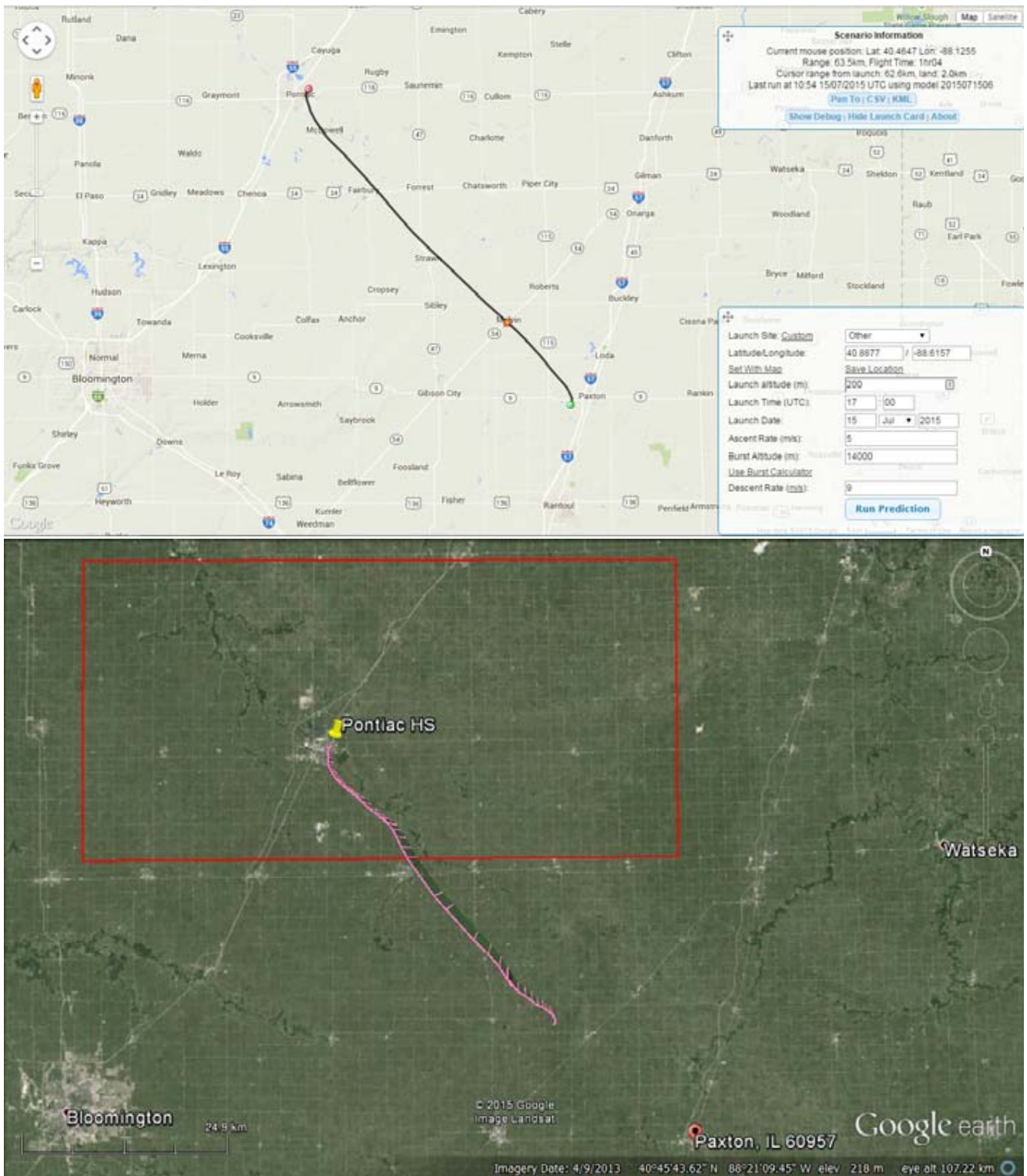
Figure 3. Comparison of actual (bottom) and predicted (top) flight paths on 15 July 2015. Flights were predicted prior to launch using NOAA GFS (National Oceanic and Atmospheric Administration Global Forecast System) models. The actual flight path was tracked using a Stratostar command module. The red box in the bottom panel indicates the bounding box for the NDVI dataset.

variation of convention from Laubach and Fritsch, α_S converted the mass of the column to moles, so the final flux units were molar (μmol m^{-2} s^{-1}) instead of mass (mg m^{-2} s^{-1}). The constant mass was calculated as described in the first paragraph of Sect. 2. Essentially, a fixed mass was selected from the larger of the two flight's mixed-layer masses, as calculated from the vertical density profile and the mixed-layer height. The mixed-layer height was determined from inspection of the carbon dioxide profiles for each flight. Note that we use the term height when we reference the mixed layer, but since the data were collected via GPS, strictly speaking the vertical coordinate is altitude referenced to sea level, not height above the ground. For $\langle s \rangle_{\text{top1,2}}$, the carbon dioxide mixing ratio was averaged to the altitudes that were determined for the fixed mass. For one altitude, this is the top mixed-layer height, for the other flight, the altitude is determined from the equivalent mass calculation.

The second term on the right-hand side of Eq. (2) accounts for synoptic-scale subsidence. The subsidence velocity (w_{top}) was determined from the National Center for Environmental Prediction's North American Regional Reanalysis composites (http://www.esrl.noaa.gov/psd/cgi-bin/data/narr/plothour.pl). Omega (Pa s^{-1}) at 70 kPa and 18:00 GMT was converted to a vertical velocity using the air temperature from the same data source, the ideal gas law and the hydrostatic equation ($w_{\text{top}} = -\Omega/(\rho g)$). The density ($\rho_{\text{top}}$) was calculated by averaging the density at the top of the mixed-layer mass for the two flights. The Δs term depends on the averaged carbon dioxide mixing ratio and the mixing ratio just above the height of the fixed mass. The next 250 m of height were averaged to determine s_{top}. Since I_S^G is the integrated ground flux, it was divided by the time between the two flights to produce an averaged ground flux (that is, NEE). The sign convention for the exchange was relative to the atmosphere, so net uptake by the crops (photosynthesis exceeds respiration) was negative.

The time series of NEE measurements was then compared to NDVI values obtained from the Terra MODIS satellite. The NDVI values (Vegetation Indices 16-Day L3 Global 1km, MOD13A2) were retrieved from Reverb/ECHO, courtesy of the NASA EOSDIS Land Processes Distributed Active Archive Center (LP DAAC), USGS/Earth Resources Observation and Science (EROS) Center, Sioux Falls, South Dakota (http://reverb.echo.nasa.gov/). The online version of the HDF-EOS To GeoTIFF Conversion Tool (HEG) was used to retrieve a subset (upper-left corner: 41.084° N, 88.977° W; lower-right corner: 40.770° N, 88.121° W) of NDVI values as a GeoTIFF file, which were then averaged with R to produce one NDVI value for the area per 16-day period. This provided one NDVI value for each 16-day period from April 2014 to December 2015. The seasonal trends in NDVI and NEE were then compared.

NEE values from the HAB methodology were also compared to data from an EC tower site located in Bondville, IL (Meyers and Hollinger, 2004), that is part of the Ameri-

Flux network (site US-Bo1; Baldocchi et al., 2001). Previous studies at this site have assessed how agricultural systems contribute to atmospheric carbon balance (Hollinger et al., 2005; West et al., 2010). Half-hour flux data from 1996 to 2008 were averaged for daytime values between 11:00 and 15:00 (central standard time) to correspond to HAB launch times. The data from within these times were grouped into 10-day bins based on day of year, and averages and standard deviations were calculated across the entire 13-year data set to produce a composite seasonal cycle. Using the composite seasonal cycle allows individual NEE estimates from the HAB experiment to be compared to the expected variability for the same day of the year.

3 Results and discussion

The observed vertical profiles of carbon dioxide and associated NEE values (Fig. 4) often exhibited characteristics of the ideal flight (Fig. 1), but there was more variation and some flights exhibited more complexity. Many flights had a sharp decrease in carbon dioxide mixing ratios that corresponded to a well-defined boundary layer height. For example, the second flight on 14 August 2014 had a boundary layer height that increased by approximately 250 m compared to the first flight (Fig. 4, top-left panel). This is consistent with the growth in the boundary layer over a 3 h period (Stull, 1988, Fig. 1.7). Above around 1800 m, carbon dioxide mixing ratios between the two flights approximately matched, as expected. For the flights on 13 August 2015, the carbon dioxide mixing ratios observed within the mixed layer showed near-ideal behavior (Fig. 4, top-right panel). In this case, both a decrease in carbon dioxide mixing ratio within the mixed layer and an increase in the boundary layer height were observed. However, above the transition, there is a difference in mixing ratios that cannot be unequivocally assigned to local surface exchange. The calculated positive contribution to NEE from approximately 1500 to 2400 m could be attributed to entrainment processes and therefore would be considered as part of the surface exchange. The more complex structure of the profile observed during the first flight could be attributed to a residual mixed layer from the previous day. Alternatively, the increase in carbon dioxide mixing ratios could be due to long-range transport and changes in the source regions of the free-tropospheric winds. This would be a violation of our assumption of spatial homogeneity and should not be included in the surface NEE summation. Our current analysis includes this contribution, but additional information about boundary layer structure (for example, profiles of temperature and humidity) could resolve this question.

There was an instrumentation issue with a different carbon dioxide sensor used on three flights: 19 June, 2 July and 15 July 2015. Instead of the LI-820 sensor which only measured carbon dioxide, the LI-840 was deployed that measured both carbon dioxide and water vapor. The intent was to
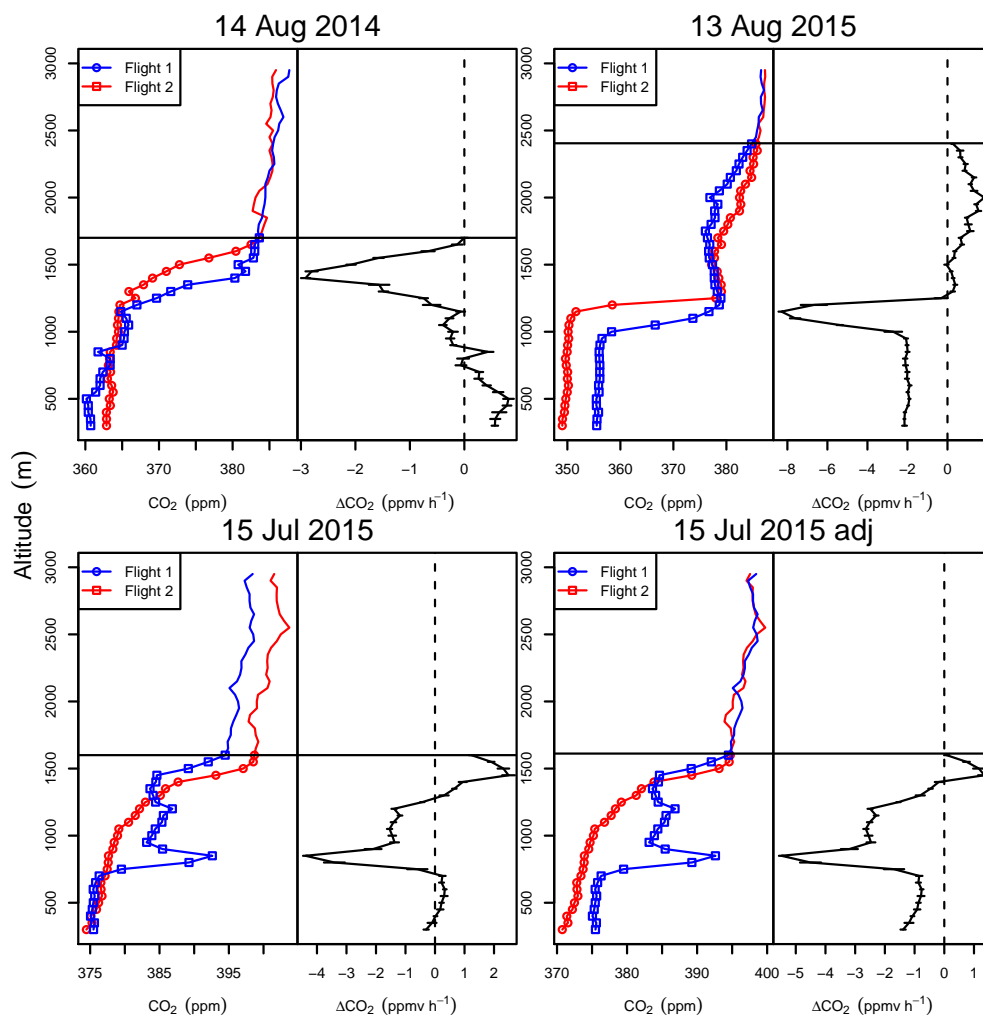
Figure 4. The left portion of each panel shows the mixing ratio of carbon dioxide to an altitude of 3000 m for the two launches (blue for the first launch, red for the second). The differences in carbon dioxide mixing ratio contribute to the calculated NEE and also help to visualize mixed-layer processes (ΔCO_2). The error bars for ΔCO_2 are 1 standard error. The top-left panel from 14 August 2014 shows a flight that has little change in the mixed-layer carbon dioxide mixing ratio, but the increase in boundary layer height leads to negative values for ΔCO_2 and hence a negative NEE. The top-right panel from 13 August 2015 shows a flight that has both a decrease in mixed-layer carbon dioxide mixing ratio and an increase in the boundary layer height, contributing to a negative NEE. However, there is also a positive ΔCO_2 above the mixed layer that is not straightforward to interpret (see text). The bottom panels from 15 July 2015 demonstrate a flight that was corrected due to instrumentation error. The original data (bottom-left) had carbon dioxide mixing ratios that differed consistently in the free troposphere. This was corrected to match free-tropospheric carbon dioxide mixing ratios between flights and produced reasonable profiles of carbon dioxide mixing ratio and ΔCO_2 in the boundary layer (bottom-right).

gain additional information about the boundary layer structure from the water vapor profile. However, with this new instrument, carbon dioxide mixing ratios in the free troposphere systematically differed between flights, unlike all the other flights where they were closely matched. Mixing ratios of carbon dioxide for the second flight were consistently 4 ppmv higher than the first flight, which is a factor of approximately 1 % of the total mixing ratio. We speculate that there was an error with the internal pressure sensor of the LI-840. Given this empirical observation, the data were adjusted by reducing both the recorded carbon dioxide mixing ratio and pressure values by 1 % for the second flight (Fig. 4, bottom two panels). After the adjustment, the data matched the conceptual model, which has equivalent carbon dioxide mixing ratios in the free troposphere. This procedure was applied to all three dates that used the LI-840 instrument. With the adjustment, the profile from 15 July 2015 could be interpreted as having a residual boundary layer at 1000–1300 m (Fig. 4, bottom-right panel).

3.1 Comparison of HAB results with other data sources

Our observations of NEE seasonal trends mostly matched our expectations derived from NDVI satellite values and a nearby EC site in Bondville, Illinois. In 2014, HAB NEE values were most negative in mid July ($-22.1\,\mu\text{mol}\,\text{m}^{-2}\,\text{s}^{-1}$) and became more positive as the summer went on (Fig. 5). In 2015, there was a minimum on 13 August 2015 (day of year 225) at $-27.3\,\mu\text{mol}\,\text{m}^{-2}\,\text{s}^{-1}$ and a maximum on 9 September 2015 (day of year 255) of $-5.0\,\mu\text{mol}\,\text{m}^{-2}\,\text{s}^{-1}$, and there was more variability compared to 2014. For 2014, there are only four HAB measurements and therefore only limited conclusions about the annual cycle can be drawn, but the timing of their minimum and maximum match within the 10-day averaging window of the EC values (Fig. 5). While the HAB maximum for 2015 is consistent with the EC trend, the HAB minimum occurs much later (day of year 255 vs. 205). Further research with more measurement dates is necessary to determine if the variability observed in 2015 was due to experimental imprecision or intrinsic variability in NEE. One possibility is that the sensor correction used for three flights in 2015 introduced experimental error that obscured the seasonal trend in HAB NEE. While the empirical correction produced free-tropospheric carbon dioxide mixing ratios that matched between the two flights, we do not understand the nature of the instrument malfunction and therefore we cannot assess its potential impact on the corrected NEE values.

An inspection of NDVI values (Fig. 5) does not reveal any obvious differences between 2014 and 2015 that would account for increased variability in 2015. Lower NDVI values in 2015 could reflect increased plant stress, but this is speculative. NDVI values reach their fall minimum later than the HAB NEE become positive (net respiration), but this is also true for the comparison with the long-term EC NEE values from Bondville. The timing of the fall decrease in our NDVI values is roughly consistent with seasonal NDVI trends from an agricultural area of Nebraska (Eastman et al., 2013). The lag between NEE and NDVI decreases could be due to the time that crops spend in the field before harvest. In late summer and fall, crops do not have a positive net photosynthesis, but agricultural practice is to leave crops in place to dry out. NDVI might continue to sense vegetation when crops are present in the field even if they are not undergoing photosynthesis due to senescence.

Our results are consistent in magnitude with smaller-scale measurements from the Bondville flux site. The other HAB NEE measurements are either within or very close to within 1 standard deviation of the long-term (13-year) mean of the EC data (Fig. 5). Finally, the overall seasonal trends from both 2014 and 2015 and the magnitude of the values are consistent with the trends and the range of observed data collected using the first-generation approach from 2012 to 2013 (Pocs, 2014).
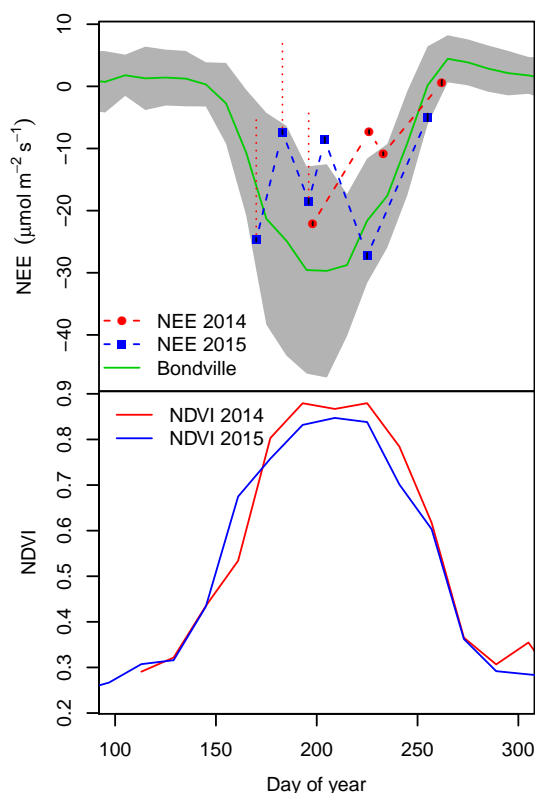
Figure 5. Seasonal patterns in NDVI (bottom panel) and NEE (top panel) for 2014 and 2015 and data from the Bondville eddy flux site for 1996 to 2008. NEE data in the top panel include the NEE HAB estimates (dashed lines and filled circles (2014) and squares (2015)) and 10-day averages of midday (11:00–15:00 local standard time) NEE for Bondville (green solid line). The gray shaded region indicates 1 standard deviation above and below the mean for Bondville. The vertical black lines are ± 1 standard error for the HAB NEE estimates. The vertical red dotted lines show the instrument adjustment that was necessary for three of the flights. HAB-based NEE falls within or very close to the shaded region. NDVI generally tracks NEE well, but NEE from both Bondville and the HAB technique approaches zero sooner than NDVI in the fall.

3.2 Error analysis

Broadly, errors in estimating NEE with the HAB methodology using the fixed-mass column approach can be separated into two categories. First, there are instrumentation errors associated with measuring the carbon dioxide mixing ratio and pressure vertical profiles. Included in this first category of error is the assumption of a constant potential temperature. Second, there are errors associated with the assumptions intrinsic to the fixed-mass column approach. In particular, the issue of horizontal advection is a challenge for a Eulerian column measurement. Because of the relatively large number of measurements, the impact of random instrument error is small. Given the ascent rates in Table 1, the 1 Hz instrument output rate and the bin height of 50 m, each bin has 7–10 dif-

ferent measurements of carbon dioxide mixing ratio. Assuming that mixing ratios should be constant within a 50 m bin, the standard error for the ΔCO_2 for each bin (also assuming errors are not correlated) is given in Fig. 4 (right-side of each panel). Propagating these errors to the NEE estimate leads to the conclusion that random errors are not significant. Visually, the standard errors are smaller than the plotting characters in Fig. 5 and all are less than $0.7 \, \mu mol \, m^{-2} \, s^{-1}$. The statistical errors associated with assuming a constant potential temperature are also small. The r^2 value exceeded 0.999 for all of the linear fits. Systematic measurement error could potentially be much larger. Examining the first term on the right-hand side of Eq. (2), errors in estimating the mass of the column scale linearly. For example, a 1 % error in the pressure measurement would translate into a roughly 1 % error in the column mass, which is small. In contrast, the calculation of surface exchange depends of the difference of the two averaged carbon dioxide mixing ratios. If there were an error of 1 % from one flight to the next, there would be a large error in the difference. That this error is relatively minimal is seen in the good match of the carbon dioxide mixing ratios above the mixed layer. For example, the match above 2500 m for 13 August 2015 (Fig. 4) is very good and is typical of most of the flights.

Another source of potential error is that the air measured by the carbon dioxide instrument was not dried. Since the mixing ratio output of the instrument depends on the measured air pressure, a flux of water vapor into the boundary layer will lead to a bias. This error can be assessed by assuming a typical evapotranspiration flux of water vapor and using the boundary layer height of 1500 m from the 14 August 2014 flight (Fig. 4). This simple treatment ignores boundary layer growth and the entrainment of drier air from the free troposphere, so it is a upper bound on the error. Using a typical corn–soy crop evapotranspiration rate of $0.70 \, mm \, h^{-1}$ gives an integrated flux into the column of 2.1 kg of water vapor over 3 h, the typical flight time. On 14 August 2014, the column mass was approximately 1500 kg, and accounting for the differences in the molecular masses of air and water vapor gives a pressure impact of 0.23 %. Assuming the error in the carbon dioxide mixing ratio is linear with small changes in pressure and using a mixing ratio of 365 ppmv and again the flight time of 3 h, the effect on ΔCO_2 would be approximately $0.28 \, ppmv \, h^{-1}$. For this upper-bound error estimate, the effect would be $4 \, \mu mol \, m^{-2} \, s^{-1}$ for the 14 August 2014 flight. This points out the need to understand this effect more fully in future measurement campaigns and demonstrates our motivation to use an instrument that measures water vapor.

Horizontal advection is a potential source of error with the assumptions of the fixed-mass column approach. To consider errors associated with advection in the mixed layer, back trajectories were calculated for each flight day. Details are given in the Supplement, but due to the relatively short time between flights (3 h), changes in the source regions were small.

Given the homogeneous landscape of the Midwestern corn–soy rotation, the potential error due to advection within the mixed layer is minimized. Laubach and Fritsch (2002) examined the role of advection above the mixed layer using the subsidence velocity and mixing ratio profiles, and they found the contribution to be small in most cases. They judged the correction to be "often not worthwhile" but did note some exceptions. As noted below, an advantage of the HAB methodology is its low cost. This opens the possibility to use multiple systems on the same day, which could be done along a wind transect to assess the role of horizontal advection in a quantitative way.

3.3 Advantages and limitations of the HAB methodology

The HAB methodology has numerous advantages. (1) It is a direct mass-balance approach. There are no assumptions necessary to calculate the surface exchange: the equations rely only on the ideal gas law. (2) Using a single instrument to measure both carbon dioxide vertical profiles reduces errors inherent in difference measurements. By comparing the two carbon dioxide profiles retrieved above the mixed layer, issues associated with sensor imprecision between flights can be assessed. This allowed us to spot problems with the LI-840 instrument compared to the more stable LI-820. (3) The HAB methodology measures NEE at an intermediate scale between stationary eddy flux sites and regional-scale measurements derived from satellite inversions of remotely sensed carbon dioxide concentrations. (4) The costs associated with HAB are modest compared to aircraft flux measurements. This lowers the barrier for entry and opens the possibility for citizen science groups to contribute measurements. For example, high school students have observed and assisted our launches.

There are some drawbacks. Most importantly, conducting balloon launches is time intensive and measurements are episodic. Unlike the continuous half-hour data stream from an EC tower, measurements need to be acquired by hand. Because of this, the method is useful for temporally limited comparisons to other data sources as done in the current study, but they would increase is not appropriate for calculating annual net NEE values by itself.

Like the EC method of determining surface fluxes (Horst and Weil, 1992), another issue is determining the spatial extent of the surface area (footprint) that influences the NEE calculated by the HAB methodology. A simple scaling analysis gives an approximate upwind footprint distance based on vertical mixing times and horizontal wind speeds throughout the mixed layer. Using the definition of the mixed layer of Stull (1988) as the region of the atmosphere in contact with the surface within the times scale of 1 h, a typical upper-end horizontal wind speed ($16 \, km \, h^{-1}$) gives a upwind length scale of 16 km. An upper limit for the upwind footprint distance that does not rely on this definition would use the time

between flights (4 h maximum) and the same wind speed to get a distance of 64 km. A more detailed study of turbulent mixing would be necessary to assess the footprint extent perpendicular to the horizontal wind direction. The necessity for a spatially homogeneous landscape limits the locations for deployment. Even if this condition is met, forested landscapes, urban areas and private property pose an issue for instrument retrieval. A tethered balloon system would address this problem, but increase the complexity of the experiment.

4 Conclusions

Further research with the HAB methodology could be done to extend the validity of the method. Multiple launches could be conducted on the same day in different locations, which would help assess the spatial footprint of the HAB methodology. A series of more than two launches performed on one day at the same location would allow diurnal cycles in NEE to be considered. Both of these improvements require multiple launch teams, which could be used as an opportunity to recruit citizen scientists into the process. The AirCore approach (Karion et al., 2010) will also be considered, since multiple citizen scientist teams could use this low-cost sampling method, with analysis taking place at a central laboratory. The launch site could be moved to a more agricultural landscape, which could minimize the influence of local anthropogenic sources potentially in Pontiac. The methodology would also provide useful information for regional-scale inversion estimates (Gourdji et al., 2012) that could account for the advective component of the observed carbon dioxide profiles.

Because of the massive human perturbation of the natural carbon cycle due to agriculture, landscape-scale measurements are necessary to understand the fully integrated surface exchanges. While small-scale eddy flux measurements are a good tool for assessing particular agricultural practices at the plot scale, the HAB methodology can be used to verify carbon dioxide exchanges over much larger spatial scales. Agriculture occupies a vast amount of land, so understanding its ability to take up or release carbon dioxide is crucial for understanding the global carbon cycle as a whole.

5 Data availability

For this initial exploration of the HAB methodology, the datasets are available upon request from the corresponding author. In the future, all data generated by citizen scientists will be open access.

Three external sources of data were used in this analysis. Vertical velocities were derived from the NCEP reanalysis (http://www.esrl.noaa.gov/psd/cgi-bin/data/narr/plothour.pl) (NOAA, 2016a). The NDVI values from MODIS came from the Reverb/ECHO tool (http://reverb.echo.nasa.gov/) (NASA, 2016). The EC flux data were from the Ameriflux

network server (http://ameriflux.lbl.gov/data/download-data/?site_id=US-Bo1) (AmeriFlux, 2016). In addition, NOAA reanalysis data were used for the trajectories calculated in the Supplement (ftp://arlftp.arlhq.noaa.gov/pub/archives) (NOAA, 2016b).

The Supplement related to this article is available online at doi:10.5194/amt-9-5707-2016-supplement.

References

AmeriFlux: AmeriFlux data, available at: http://ameriflux.lbl.gov/data/download-data/?site_id=US-Bo1, last access: 28 November 2016.

Baldocchi, D., Falge, E., Gu, L., Olson, R., Hollinger, D., Running, S., Anthoni, P., Bernhofer, C., Davis, K., Evans, R., Fuentes, J., Goldstein, A., Katul, G., Law, B., Lee, X., Malhi, Y., Meyers, T., Munger, W., Oechel, W., Paw, K. T., Pilegaard, K., Schmid, H. P., Valentini, R., Verma, S., Vesala, T., Wilson, K., and Wofsy, S.: FLUXNET: a new tool to study the temporal and spatial variability of ecosystem-scale carbon dioxide, water vapor, and energy flux densities, B. Am. Meteorol. Soc., 82, 2415–2434, doi:10.1175/1520-0477(2001)082<2415:FANTTS>2.3.CO;2, 2001.

Barcza, Z., Kern, A., Haszpra, L., and Kljun, N.: Spatial representativeness of tall tower eddy covariance measurements using remote sensing and footprint analysis, Agr. Forest Meteorol., 149, 795–807, doi:10.1016/j.agrformet.2008.10.021, 2009.

Chou, W. W., Wofsy, S. C., Harriss, R. C., Lin, J. C., Gerbig, C., and Sachse, G. W.: Net fluxes of CO_2 in Amazonia derived from aircraft observations, J. Geophys. Res.-Atmos., 107, ACH 4–1–ACH 4–15, 4614, doi:10.1029/2001JD001295, 2002.

Churkina, G., Schimel, D., Braswell, B. H., and Xiao, X.: Spatial analysis of growing season length control over net ecosystem exchange, Glob. Change Biol., 11, 1777–1787, doi:10.1111/j.1365-2486.2005.001012.x, 2005.

Ciais, P., Sabine, C., Bala, G., Bopp, L., Brovkin, V., Canadell, J., Chhabra, A., DeFries, R., Galloway, J., Heimann, M., Jones, C., Le Quere, C., Myneni, R., Piao, S., and Thornton, P.: Carbon and other biogeochemical cycles, book section 6, 465–570, Cambridge University Press, Cambridge, UK and New York, USA, doi:10.1017/CBO9781107415324.015, 2013.

Denmead, O., Raupach, M., Dunin, F., Cleugh, H., and Leuning, R.: Boundary layer budgets for regional estimates of scalar fluxes, Glob. Change Biol., 2, 255–264, doi:10.1111/j.1365-2486.1996.tb00077.x, 1996.

Eastman, J. R., Sangermano, F., Machado, E. A., Rogan, J., and Anyamba, A.: Global trends in seasonality of normalized difference vegetation index (NDVI), 1982–2011, Remote Sensing, 5, 4799, doi:10.3390/rs5104799, 2013.

Enting, I. G., Trudinger, C. M., and Francey, R. J.: A synthesis inversion of the concentration and $\delta^{13}C$ of atmospheric CO_2, Tellus B, 47, 35–52, doi:10.1034/j.1600-0889.47.issue1.5.x, 1995.

Gourdji, S. M., Mueller, K. L., Yadav, V., Huntzinger, D. N., Andrews, A. E., Trudeau, M., Petron, G., Nehrkorn, T., Eluszkiewicz, J., Henderson, J., Wen, D., Lin, J., Fischer, M., Sweeney, C., and Michalak, A. M.: North American CO_2 exchange: inter-comparison of modeled estimates with results from a fine-scale atmospheric inversion, Biogeosciences, 9, 457–475, doi:10.5194/bg-9-457-2012, 2012.

Guan, K., Berry, J. A., Zhang, Y., Joiner, J., Guanter, L., Badgley, G., and Lobell, D. B.: Improving the monitoring of crop productivity using spaceborne solar-induced fluorescence, Glob. Change Biol., 22, 716–726, doi:10.1111/gcb.13136, 2016.

Gurney, K. R., Law, R. M., Denning, A. S., Rayner, P. J., Baker, D., Bousquet, P., Bruhwiler, L., Chen, Y.-H., Ciais, P., Fan, S., Fung, I. Y., Gloor, M., Heimann, M., Higuchi, K., John, J., Maki, T., Maksyutov, S., Masarie, K., Peylin, P., Prather, M., Pak, B. C., Randerson, J., Sarmiento, J., Taguchi, S., Takahashi, T., and Yuen, C.-W.: Towards robust regional estimates of CO_2 sources and sinks using atmospheric transport models, Nature, 415, 626–630, doi:10.1038/415626a, 2002.

Gurney, K. R., Law, R. M., Denning, A. S., Rayner, P. J., Pak, B. C., Baker, D., Bousquet, P., Bruhwiler, L., Chen, Y.-H., Ciais, P., Fung, I. Y., Heimann, M., John, J., Maki, T., Maksyutov, S., Peylin, P., Prather, M., and Taguchi, S.: Transcom 3 inversion intercomparison: Model mean results for the estimation of seasonal carbon sources and sinks, Global Biogeochem. Cy., 18, gB1010, doi:10.1029/2003GB002111, 2004.

Hollinger, S. E., Bernacchi, C. J., and Meyers, T. P.: Carbon budget of mature no-till ecosystem in North Central Region of the United States, Agr. Forest Meteorol., 130, 59–69, doi:10.1016/j.agrformet.2005.01.005, 2005.

Horst, T. W. and Weil, J. C.: Footprint estimation for scalar flux measurements in the atmospheric surface layer, Bound.-Lay. Meteorol., 59, 279–296, doi:10.1007/BF00119817, 1992.

Karion, A., Sweeney, C., Tans, P., and Newberger, T.: AirCore: An innovative atmospheric sampling system, J. Atmos. Ocean. Tech., 27, 1839–1853, doi:10.1175/2010JTECHA1448.1, 2010.

Krausmann, F., Erb, K.-H., Gingrich, S., Haberl, H., Bondeau, A., Gaube, V., Lauk, C., Plutzar, C., and Searchinger, T. D.: Global human appropriation of net primary production doubled in the 20th century, P. Natl. Acad. Sci. USA, 110, 10324–10329, doi:10.1073/pnas.1211349110, 2013.

Laubach, J. and Fritsch, H.: Convective boundary layer budgets derived from aircraft data, Agr. Forest Meteorol., 111, 237–263, doi:10.1016/S0168-1923(02)00038-2, 2002.

Luo, Z., Wang, E., and Sun, O. J.: Can no-tillage stimulate carbon sequestration in agricultural soils? A meta-analysis of paired experiments, Agr. Ecosyst. Environ., 139, 224–231, doi:10.1016/j.agee.2010.08.006, 2010.

Martins, K. D., Sweeney, C., Stirm, B. H., and Shepson, P. B.: Regional surface flux of CO_2 inferred from changes in the advected CO_2 column density, Agr. Forest Meteorol., 149, 1674–1685, doi:10.1016/j.agrformet.2009.05.005, 2009.

Mays, K. L., Shepson, P. B., Stirm, B. H., Karion, A., Sweeney, C., and Gurney, K. R.: Aircraft-based measurements of the carbon footprint of Indianapolis, Environ. Sci. Technol., 43, 7816–7823, doi:10.1021/es901326b, 2009.

Meyers, T. P. and Hollinger, S. E.: An assessment of storage terms in the surface energy balance of maize and soybean, Agr. Forest Meteorol., 125, 105–115, doi:10.1016/j.agrformet.2004.03.001, 2004.

Mkhabela, M. S., Mkhabela, M. S., and Mashinini, N. N.: Early maize yield forecasting in the four agro-ecological regions of Swaziland using NDVI data derived from NOAA's-AVHRR, Agr. Forest Meteorol., 129, 1–9, doi:10.1016/j.agrformet.2004.12.006, 2005.

Monson, R. and Baldocchi, D.: Terrestrial Biosphere-Atmosphere Fluxes, Cambridge University Press, ISBN-13: 978-1-107-04065-6, Cambridge, UK, 2014.

NASA: MODIS data, available at: http://reverb.echo.nasa.gov/, last access: 28 November 2016.

NOAA: NCEP data, available at: http://www.esrl.noaa.gov/psd/cgi-bin/data/narr/plothour.pl, last access: 28 November 2016a.

NOAA: NCEP/NCAR Reanalysis data, available at: ftp://arlftp.arlhq.noaa.gov/pub/archives/, last access: 28 November 2016b.

Peters, W., Jacobson, A. R., Sweeney, C., Andrews, A. E., Conway, T. J., Masarie, K., Miller, J. B., Bruhwiler, L. M. P., Petron, G., Hirsch, A. I., Worthy, D. E. J., van der Werf, G. R., Randerson, J. T., Wennberg, P. O., Krol, M. C., and Tans, P. P.: An atmospheric perspective on North American carbon dioxide exchange: CarbonTracker, P. Natl. Acad. Sci. USA, 104, 18925–18930, doi:10.1073/pnas.0708986104, 2007.

Pocs, M.: A high-altitude balloon platform for exploring the terrestrial carbon cycle, DePaul Discoveries, 3, Article 2, http://via.library.depaul.edu/depaul-disc/vol3/iss1/2/ (last access: 14 November 2016), 2014.

Poeplau, C. and Don, A.: Carbon sequestration in agricultural soils via cultivation of cover crops – A meta-analysis, Agr. Ecosyst. Environ., 200, 33–41, doi:10.1016/j.agee.2014.10.024, 2015.

Potosnak, M. J., Wofsy, S. C., Denning, A. S., Conway, T. J., Munger, J. W., and Barnes, D. H.: Influence of biotic exchange and combustion sources on atmospheric CO_2 concentrations in New England from observations at a forest flux tower, J. Geophys. Res.-Atmos., 104, 9561–9569, doi:10.1029/1999JD900102, 1999.

Potter, C., Klooster, S., Huete, A., and Genovese, V.: Terrestrial carbon sinks for the United States predicted from MODIS satellite data and ecosystem modeling, Earth Interact., 11, 1–21, doi:10.1175/EI228.1, 2007.

R Core Team: R: A Language and Environment for Statistical Computing, R Foundation for Statistical Computing, Vienna, Austria, https://www.R-project.org/, last access: 14 November 2016.

Reuter, M., Buchwitz, M., Hilker, M., Heymann, J., Schneising, O., Pillai, D., Bovensmann, H., Burrows, J. P., Bösch, H., Parker, R., Butz, A., Hasekamp, O., O'Dell, C. W., Yoshida, Y., Gerbig, C., Nehrkorn, T., Deutscher, N. M., Warneke, T., Notholt, J., Hase, F., Kivi, R., Sussmann, R., Machida, T., Matsueda, H., and Sawa, Y.: Satellite-inferred European carbon sink larger than expected,

Atmos. Chem. Phys., 14, 13739–13753, doi:10.5194/acp-14-13739-2014, 2014.

Schneising, O., Heymann, J., Buchwitz, M., Reuter, M., Bovensmann, H., and Burrows, J. P.: Anthropogenic carbon dioxide source areas observed from space: assessment of regional enhancements and trends, Atmos. Chem. Phys., 13, 2445–2454, doi:10.5194/acp-13-2445-2013, 2013.

Sims, D. A., Rahman, A. F., Cordova, V. D., El-Masri, B. Z., Baldocchi, D. D., Bolstad, P. V., Flanagan, L. B., Goldstein, A. H., Hollinger, D. Y., Misson, L., Monson, R. K., Oechel, W. C., Schmid, H. P., Wofsy, S. C., and Xu, L.: A new model of gross primary productivity for North American ecosystems based solely on the enhanced vegetation index and land surface temperature from MODIS, Remote Sens. Environ., 112, 1633–1646, doi:10.1016/j.rse.2007.08.004, 2008.

Stull, R.: An Introduction to Boundary Layer Meteorology, Atmospheric Science Library, Springer, ISBN-10: 90-277-2769-4, Dordrecht, the Netherlands, 1988.

Sus, O., Heuer, M. W., Meyers, T. P., and Williams, M.: A data assimilation framework for constraining upscaled cropland carbon flux seasonality and biometry with MODIS, Biogeosciences, 10, 2451–2466, doi:10.5194/bg-10-2451-2013, 2013.

West, T. O., Brandt, C. C., Baskaran, L. M., Hellwinckel, C. M., Mueller, R., Bernacchi, C. J., Bandaru, V., Yang, B., Wilson, B. S., Marland, G., Nelson, R. G., Ugarte, D. G. D. L. T., and Post, W. M.: Cropland carbon fluxes in the United States: increasing geospatial resolution of inventory-based carbon accounting, Ecol. Appl., 20, 1074–1086, doi:10.1890/08-2352.1, 2010.

Wofsy, S. C., Harriss, R. C., and Kaplan, W. A.: Carbon dioxide in the atmosphere over the Amazon Basin, J. Geophys. Res.-Atmos., 93, 1377–1387, doi:10.1029/JD093iD02p01377, 1988.